ACS APPLIED MATERIALS & INTERFACES

Research Article

www.acsami.org

Synthesis of 3D-Nanonet Hollow Structured Co_3O_4 for High Capacity Supercapacitor

Yanyan Wang,[†] Ying Lei,[†] Jing Li,[‡] Li Gu,[‡] Hongyan Yuan,[†] and Dan Xiao*[,†,‡]

[†]College of Chemical Engineering and [‡]College of Chemistry, Sichuan University, 29 Wangjiang Road, Chengdu 610064, People's Republic of China

Supporting Information

ABSTRACT: A 3D-nanonet structured cobalt-basic-carbonate precursor has been obtained by a facile, low cost and eco-friendly route under ambient temperature and pressure. After calcination in air, the as-prepared precursor was converted to a 3D-nanonet hollow structured Co_3O_4 with its original frame structure almost preserved. Encouragingly, by alternating experimental parameters (Table S1 in the Supporting Information), such as concentration of the starting reagents and calcination temperature, we got the optimized condition for the final product with desirable electrochemical performance (Figure S1 in the Supporting Information). The pseudocapacitive properties of the obtained Co_3O_4 were evaluated by cyclic voltammetry (CV), galvanostatic charge−discharge measurement and electrochemical impedance spectroscopy in 6.0 M KOH solution. At different scan rates of 5, 10, 20, and 30 mV s^{-1}, the corresponding specific capacitances were 820, 755, 693, and 656 F g^{-1}, respectively. The material also exhibited superior charge−discharge stability and maintained 90.2% of its initial capacitance after 1000 continuous charge−discharge cycles at a current density of 5 A g^{-1}. From a broad view, our research and the outstanding results not only present a feasible access to nanostructured Co_3O_4 but also remind us of paying more attention to the simple synthetic methods without complex processes and sophisticated instruments.

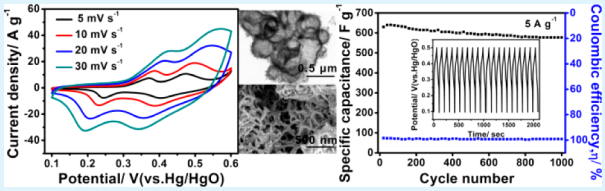

KEYWORDS: *eco-friendly, ambient temperature, hollow structured Co_3O_4, pseudocapacitive properties*

1. INTRODUCTION

Nowadays, energy problems have become the greatest focus attracting the world's attention and triggering tremendous efforts for energy storage and conversion.[1−4] Owing to long service life, high energy density, superior power density, and environmental benignity,[5] electrochemical capacitors (ECs) are chosen as an ideal energy storage system. Generally, in terms of the mechanism of charge storage, ECs can be divided into electric double-layer capacitors (EDLCs) and pseudocapacitors.[6] However, because of their large capacitance and fast redox kinetics,[7] the research of pseudocapacitors based on metal oxides and hydroxides has received considerable attention over the past decades. Among them, cobalt-based materials, including cobalt oxides and hydroxides, occupy a very critical position, due to their high theoretical capacitances (more than 3000 F g^{-1})[8] and easy processing.[9,10] Recently, numerous researchers have engaged in synthesizing nanoscaled Co_3O_4 materials,[5,10−13] which are expected to possess the desirable pseudocapacitive performance. For example, Meher et al.[12] have proposed an interesting homogeneous precipitation process under hydrothermal conditions by employing Triton X-100 as the surfactant to tailor the obtained Co_3O_4 material into an ultralayered morphology. Furthermore, Wei and co-workers[10] have also described the synthesis of Co_3O_4 with high porosity in the novel form of aerogels. In addition, Yang et al.[13] have reported an approach to a Co_3O_4 nanowire network (nanonet) coated on a carbon fiber paper. Although the reports mentioned above have achieved relatively high specific capacitances, high cost and poor safety of the processes greatly hindered the widespread use of the methods to synthesize nanostructured materials on a large scale. To overcome disadvantages of the routes mentioned above, much effort has been devoted into seeking for alternatively facile and efficient approaches to obtaining high performance Co_3O_4 materials endowed with wonderful porous nanostructure.[5,10−15] For instance, flower-like Co_3O_4 has been synthesized by a one-step, template-free and water-controlled precipitation approach.[16] Again, hollow Co_3O_4 boxes have been obtained from a facile two-step route, a low temperature recrystallization process, and the following thermal decomposition.[5] Nevertheless, the superior approaches are accompanied by unsatisfactory electrochemical properties. Obviously, it is still a great challenge to make a balance between excellent pseudocapacitive performance and facile synthetic pathway.

In our work, instead of focusing on the complex processes and sophisticated instruments, we employed a simple and easy-operating heterogeneous precipitation method to achieve the aim of preparing nanoscaled Co_3O_4. Surprisingly, the extremely conventional method gave rise to a 3D-nanonet hollow structure and unexpectedly excellent capacitive performance. Particularly, the 3D-nanonet hollow structured Co_3O_4 delivered an outstanding specific capacitance of 820 F g^{-1} at 5 mV s^{-1}.

Received: January 22, 2014
Accepted: April 21, 2014
Published: April 21, 2014

   dx.doi.org/10.1021/am500464n | ACS Appl. Mater. Interfaces 2014, 6, 6739−6747

What's more, this desirable structure exhibited an excellent rate capacity and cyclic stability, which are most likely attributed to the porous structure, providing numerous pathways for fast ion and electron transfer.[13] Most importantly, cheap raw materials, easy operation, and freedom of expensive instruments lay a foundation for the potential application of the method in scale production.

2. EXPERIMENTAL DETAILS

2.1. Materials Synthesis. Analytical grade chemicals were used as received without any further purification. 0.623 g (2.5 mM) of $Co(CH_3COO)_2{\cdot}4H_2O$ and 3.96 g (20 mM) of glucose ($C_6H_{12}O_6{\cdot}H_2O$) were dissolved in 20 mL of triply-distilled water. 0.5 g (6 mM) of $NaHCO_3$ dissolved in 25 mL of triply-distilled water was added dropwise into the former solution with gentle magnetic stirring. The reaction was kept as it was for 12 h after the latter solution was added. Then a pink purple precipitate was obtained by centrifugation with successive washing with triply-distilled water and absolute ethanol for several times. The obtained precipitate was dried in a vacuum oven at 40 °C for 4 h. To obtain the final product, the as-prepared precursor was calcined in air at 250 °C for 2 h. The yield of this method is about 71%.

2.2. Characterization. The precursor and the final product, Co_3O_4, were investigated by X-ray powder diffraction (Tongda TD-3500 X-ray powder diffractometer, Liaoning, China) operating at 30.0 kV and 20.0 mA with Cu Kα radiation (λ = 0.151 48 nm). Morphologies of all the products were observed by field emission scanning electron microscopy (FESEM) (Hitachi S-4800 field emission scanning electron microscope, Tokyo, Japan). Morphologies of the detail structures were measured with transmission electron microscopy (TEM) (FEI Tecnai G2 20 high resolution transmission electron microscope, Hillsboro, OR, USA). Thermal behaviors analysis of the materials, thermogravimetric (TGA) and differential thermal analyses (DTA), were conducted by a Henven HCT-2 thermal analyzer (Beijing, China) with a ramping rate of 5 °C min^{-1} from 20 to 600 °C, under an atmosphere of air. Fourier transform infrared spectrscopy (FTIR) analysis was performed on a Thermo Scientific Nicolet 6700 FTIR spectrometer (Sugar Land, TX, USA). The Brunauer–Emmett–Teller (BET) specific surface area was obtained from the nitrogen (N_2) adsorption method using a Quadrasorb SI Automated Surface Area. XPS data was collected on a Kratos XSAM 800 spectrometer (Manchester, U.K.) with a Mg Kα X-ray (1253.6 eV) excitation source operating at 15 kV, a hemispherical electron energy analyzer, and a multichannel detector.

2.3. Electrochemical Measurements. The typical three-electrode system was employed to evaluate electrochemical properties of the obtained Co_3O_4. The working electrode was made by loading a mixture onto the nickel foam (NF) electrode (surface, 1.0 cm × 1.0 cm). The mixture consists of 80 wt % of electroactive material (Co_3O_4), 15 wt % of acetylene black, and 5 wt % of poly(vinylidene fluoride). *N*-Methyl-2-pyrrolidone was selected as the solvent. Before the test, the working electrode was dried at 80 °C overnight. Electrochemical impedance spectroscopy (EIS) measurements of the working electrode were conducted in a frequency range 10 kHz–10 mHz under open circuit potential, with an ac perturbation of 10 mV. All the measurements were performed on an Autolab PGSTAT 302 electrochemical workstation (Eco Chemie B.V., Amsterdam, the Netherlands), where a graphite sheet and Hg/HgO electrode serve as counter and reference electrodes, respectively.

3. RESULTS AND DISCUSSION

3.1. Characterization of the Precursor and Co_3O_4. Synthesis of the final product was realized through two steps, formation of the precursor and the following thermal decomposition. The precursor was obtained simply by adding $NaHCO_3$ aqueous solution dropwise into the mixture of $Co(CH_3COO)_2$ and glucose aqueous solution under ambient temperature and pressure.

To select a proper temperature for the subsequent calcination, TG and DTA analyses of the as-prepared precursor were employed in our study and the corresponding curves are shown in Figure 1. Obviously, there are two distinct weight loss

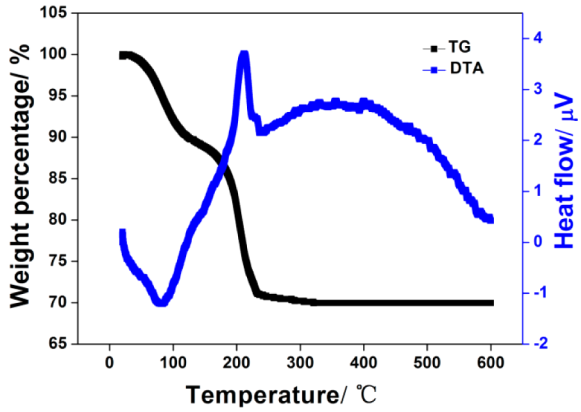

Figure 1. TG (black) and DTA (blue) profiles of the precursor.

slopes owing to dehydration and decomposition. It was found that about 11.0% weight was lost below 124 °C, corresponding to the removal of the water molecules physically adsorbed on the surface. The relatively high weight loss[5,17] of the water molecules could be attributed to the porous structure of the obtained material,[6] which was evidenced by the subsequent morphological analysis. Between 124 and 230 °C, the sharp loss of weight accompanied by an exothermic reaction is associated with the simultaneous conversion of the precursor to cobalt oxide. Up to 250 °C, the precursor almost decomposed completely. Furthermore, no obvious loss of weight was detected at higher temperatures, revealing the formation of the stable cobalt oxide. For the purpose of maintaining the porous structure and realizing the complete conversion of the precursor, 250 °C was chosen as the calcination temperature, which was further confirmed by the superior electrochemical performance (Figure S1 in the Supporting Information) of the sample obtained at this temperature.

Undergoing the decomposition process, the as-prepared precursor turned to be black powder. The XRD patterns of the precursor and the final product are displayed in Figure 2a. As presented in the black curve in Figure 2a, the XRD curve is consistent with the cubic spinel Co_3O_4 (JCPDS card no. 01-076-1802) perfectly, suggesting high purity of the obtained Co_3O_4. Peaks at 19°, 31.2°, 36.8°, 44.8°, 59.3°, and 65.2° are assigned to the (111), (220), (311), (400), (511), and (440) planes of the cubic spinel Co_3O_4, respectively. In addition, XPS patterns in Figure 2c,d further confirmed the formation of Co_3O_4. As shown in Figure 2c, we could easily observe two major peaks at binding energies of 779.72 and 794.96 eV with a spin-energy separation of 15.34 eV. The two peaks could be assigned to Co $2p_{3/2}$ and Co $2p_{1/2}$, respectively, which demonstrates the presence of a Co_3O_4 phase.[14] Futhermore, the fitting peaks at 780.9 and 796.2 eV are indexed to Co(II), whereas the peaks at 779.4 and 794.6 eV correspond to Co(III).[18] Also, in Figure 2d, the well-resolved peaks signed as O 1 and O 2 with binding energies of 529.98 and 531.35 eV correspond to the lattice oxygen of spinel Co_3O_4 and the OH species absorbed onto the surface of the obtained micro-

dx.doi.org/10.1021/am500464n | ACS Appl. Mater. Interfaces 2014, 6, 6739–6747

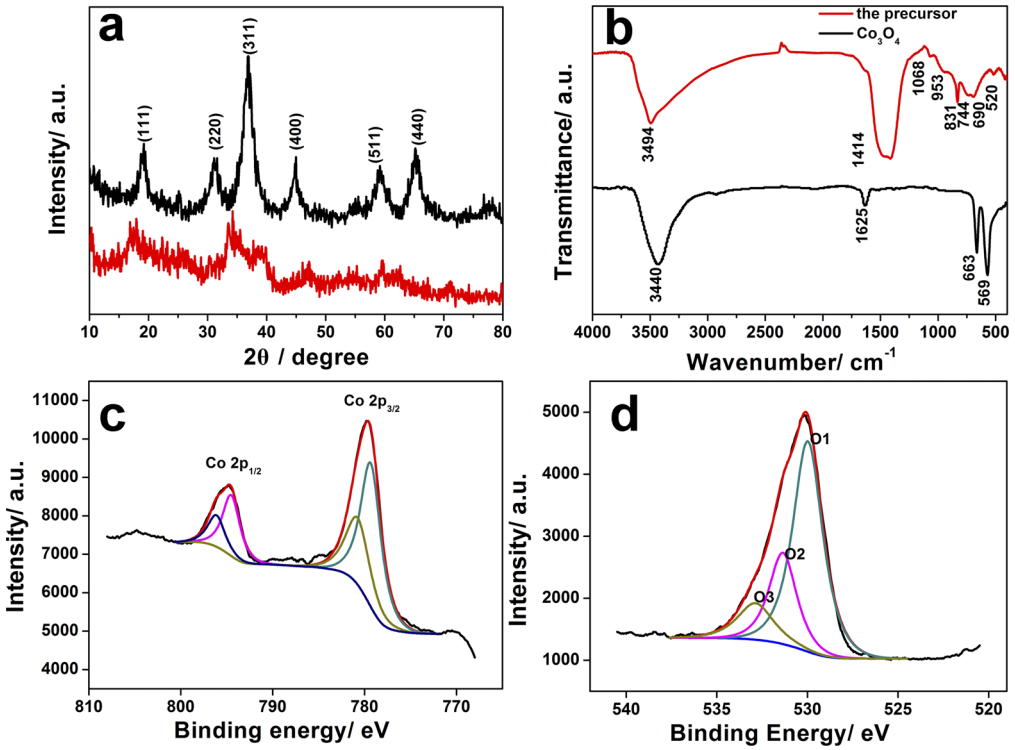

Figure 2. (a) XRD patterns of the calcined sample Co_3O_4 (black curve) and the precursor (red curve). (b) FTIR spectrum of the precursor (red curve) and Co_3O_4 (black curve). High resolution XPS measurements for the (c) Co 2p and (d) O 1s.

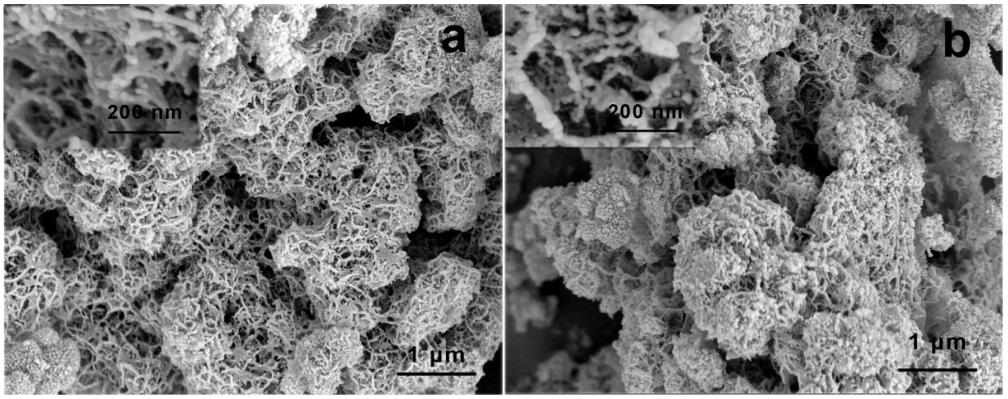

Figure 3. SEM images of (a) the precursor, (b) the as-prepared Co_3O_4. Corresponding insets illustrate higher magnification images.

structure.[19,20] The component O 3 at 532.87 eV points to multiplicity of physical absorbed and chemisorbed water near the surface.[21] Both XRD and XPS characterizations verified the complete conversion of the precursor to Co_3O_4.

However, no exact card matches well with the red curve below (in Figure 2a) presenting the crystal phase of the precursor. As shown in the curve, unremarkable diffraction peaks were observed, indicating a heterogeneous precipitation process utilized in our work.[22] For this kind of process, small size and not well crystallized samples would be obtained.

To further study the precursor and Co_3O_4 that we have obtained, FTIR analysis was carried out. As shown in the black curve in Figure 2b, sharp peaks at 663 and 569 cm^{-1} are assigned to the Co—O vibration absorption of spinel cobalt oxide.[23] In addition, peaks at 3440 and 1625 cm^{-1} could be attributed to absorbed water and surface hydroxyls are in nanocrystals' surface.[23] As presented in the red curve in Figure 2b, a strong peak at 3494 cm^{-1} belongs to the stretching vibration of O—H groups in molecular waters and hydrogen-bond O—H groups.[22] The peaks at 1414 and 831 cm^{-1} are assigned to $\nu(CO_3)$ and $\delta(CO_3)$, whereas the minor ones at 1068, 744, and 690 cm^{-1} could be attributed to ν(C═O), δ(OCO) and ρ(OCO), respectively.[24] Furthermore, the peaks at 953 and 520 cm^{-1} are ascribed to δ(Co—OH) and ρ_w(Co—OH).[22] The presence of OH^-, CO_3^{2-} groups, and structural water was evidenced by FTIR analysis. Therefore, the as-prepared precursor could be defined as cobalt-basic-carbonate compounds.

On the basis of the results obtained above and the previous reports,[22,25] we proposed a possible mechanism for the formation of the precursor and the final product, Co_3O_4. The reaction process could be expressed as

dx.doi.org/10.1021/am500464n | ACS Appl. Mater. Interfaces 2014, 6, 6739−6747

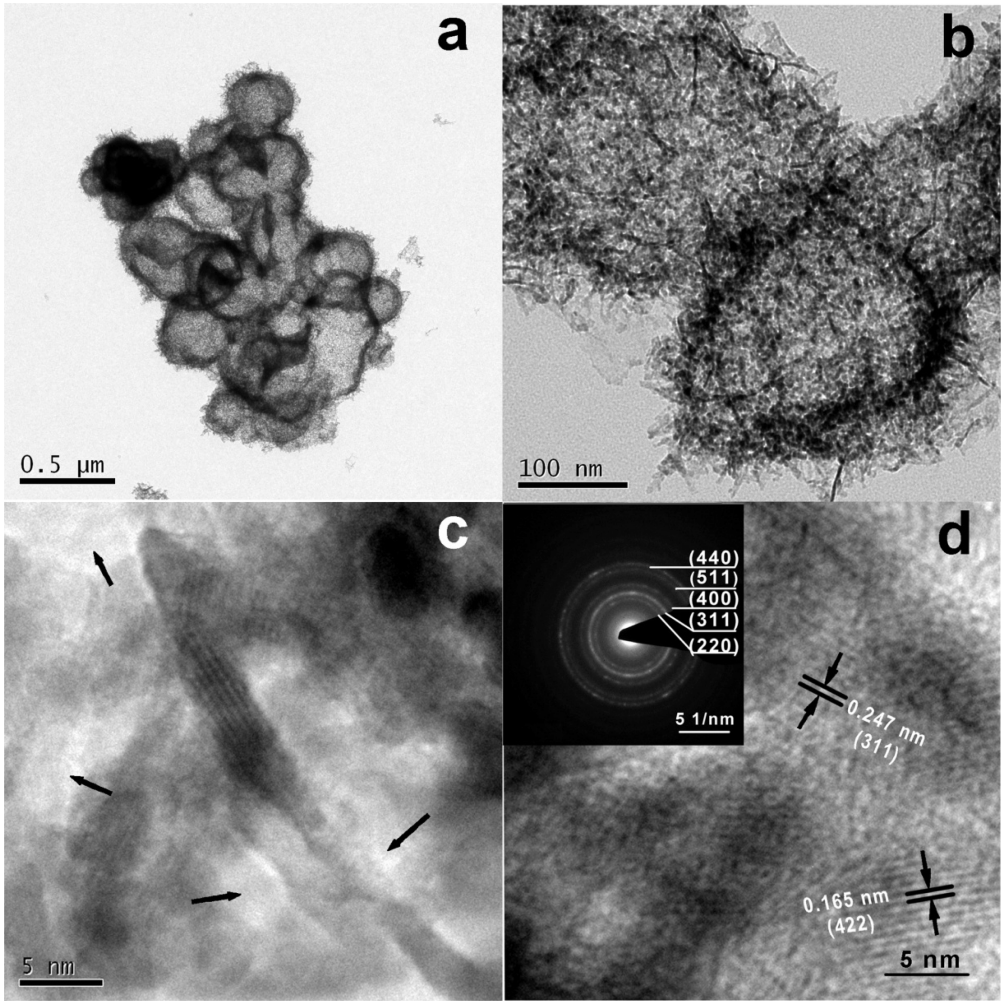

Figure 4. TEM images of Co_3O_4 at (a, b) low and (c, d) high magnification with arrows pointing to the pores in the sample. (d) HRTEM image of Co_3O_4 with the inset displaying corresponding SAED.

Scheme 1. Schematic Representation of the Possible Formation Mechanism of 3D-Nanonet Hollow Structured Co_3O_4.

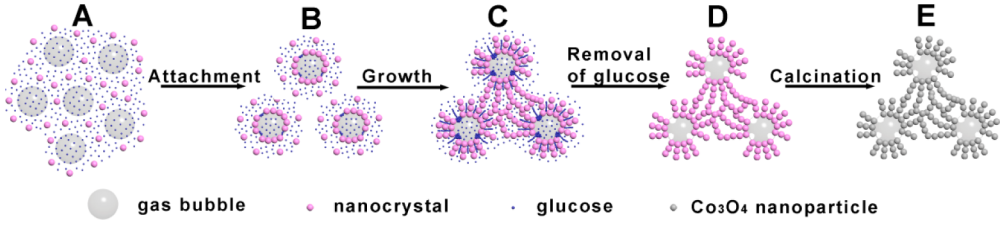

$$HCO_3^- \rightarrow H^+ + CO_3^{2-}$$

$$HCO_3^- + H_2O \rightarrow OH^- + H_2CO_3$$

$$Co^{2+} + xOH^- + 0.5(2 - x)CO_3^{2-}$$

$$+nH_2O \rightarrow Co(OH)_x(CO_3)_{0.5(2-x)}\cdot nH_2O$$

$$3Co(OH)_x(CO_3)_{0.5(2-x)}\cdot nH_2O + 0.5O_2$$

$$\rightarrow Co_3O_4 + (3n + 1.5x)H_2O + (3 - 1.5x)CO_2$$

Because morphology plays a significant role in the electrochemical properties, morphological analysis of the obtained materials was conducted by FESEM. Figure 3a,b shows the FESEM images of the precursor and Co_3O_4, respectively. We could observe the 3D-nanonet structure at first sight. Furthermore, to reveal the nanostructures more clearly, higher magnification images are presented in the corresponding insets. Through comparing Figure 3a,b, we could imply that the thermal treatment leads to the loss of some pores on the surface of the material.

To gain insight into the obtained Co_3O_4, TEM was employed in our study. As illustrated in Figure 4a, the prepared Co_3O_4 is likely to be constructed by random stacking of numerous irregular hollow spheres, which was further confirmed by the higher magnification image. As shown in Figure 4b, the size of the hollow structure is about 200 nm with a thin hairy shell of ca. 10 nm. Also, plenty of white dots scattered in Figure 4b, shown more clearly in Figure 4c, inform us of a large number of pores in the obtained Co_3O_4. Compared with the TEM images of the precursor (Figure S2 in the Supporting Information), the calcined Co_3O_4 sample

dx.doi.org/10.1021/am500464n | ACS Appl. Mater. Interfaces 2014, 6, 6739−6747

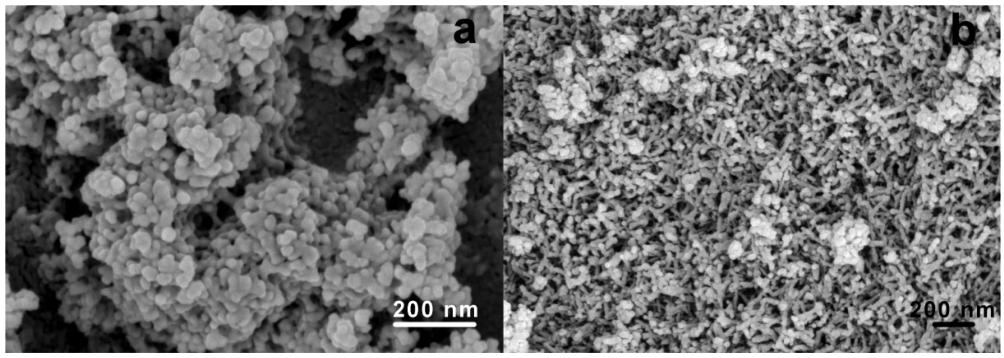

Figure 5. SEM images of (a) the initial precipitate collected from the reaction system with glucose and (b) the precursor obtained from the reaction system without glucose.

possesses a more remarkable porous structure, which is probably due to the release of gas molecules during the decomposition process. The porous structure could provide more electron/ion paths and possibly lead to superior pseudocapacitive performance.[13] A High resolution TEM (HRTEM) image and selected-area electron diffraction (SAED) pattern are depicted in Figure 4d and the corresponding inset. Interplanar distances of ca. 0.247 and 0.165 nm coincide well with the interlayer spacings of the (311) and (422) planes of the cubic Co_3O_4, respectively. In addition, well-defined rings in the SAED pattern demonstrate polycrystalline characteristics of the obtained Co_3O_4.

According to the characterization described above and the previous similar reports,[26−28] a plausible mechanism for the evolution of the 3D-nanonet hollow structured Co_3O_4 was proposed. The entire process is illustrated in Scheme 1. At the beginning, cobalt-basic-carbonate nanocrystals (Figure 5a) about 20−30 nm in diameter precipitated from the reaction system (step A). However, these nanocrystals have a tendency to aggregate. At the same time, the CO_2 gas bubbles generating from the reaction could provide the aggregation centers (step A). Because the sample obtained in the reaction system without glucose exhibits a rods-like structure (Figure 5b), we suppose that the glucose might play a role that could interfacially reinforce the gas bubbles to serve as aggregation centers. Driven by the minimization of interfacial energy, the nanocrystals aggregate around the gas−liquid interface. Then the hollow structures are formed (step B). In terms of the 3D-nanonet SEM images (Figure 3) and the fury shell of the hollow structure in the TEM images (Figures 4b and S2b, Supporting Information), the formed hollow structures might connect with each other by the nanocrystal chains through magnetic dipole−dipole attraction between the nanocrystals (step C).[29] Then remove the glucose (step D) and calcine the precursor (step E) to obtain the 3D-nanonet hollow structured Co_3O_4. In addition, the fury and discontinuous shells of the hollow structures might generate from the removal of glucose randomly aggregating around the contact surface of nanocrystals and gas bubbles.

Typically, pseudocapacitive performance of an electrode is closely associated with the distribution of pore size and the specific surface area (SSA) of the electroactive material.[30,31] Given that, BET measurement was carried out to evaluate the SSA of as-prepared porous Co_3O_4. Figure 6 displays the N_2 adsorption−desorption isotherm of the obtained Co_3O_4 measured at 77 K, with the inset presenting the corresponding pore size distribution assessed by the Barrett−Joyner−Halenda

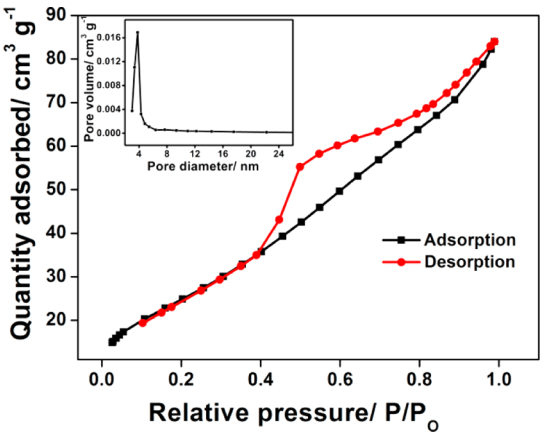

Figure 6. N_2 adsorption−desorption isotherm of the obtained Co_3O_4. The inset shows pore size distribution of the obtained Co_3O_4.

(BJH) method. As shown in Figure 6, a "type IV" hysteresis is observed, indicating that the Co_3O_4 sample mainly consists of mesopores,[12] which is further confirmed by the pore size distribution at ∼3.8 nm in the inset. In addition, the calculated SSA could reach 92.8 $m^2\ g^{-1}$, which is much higher than the previous reports[5,19] and conductive to the enhancement of electrochemical properties.[31] The uniform porosity and narrow pore size distribution falling into the optimal range (2−5 nm)[15] render our obtained Co_3O_4 nanomaterial more appropriate for supercapacitor applications.[32]

3.2. Capacitance Measurement. To investigate capacitive behavior of the electroactive material Co_3O_4, CV, EIS, and galvanostatic charge−discharge measurements were employed in our work. The CV measurements at different scan rates of 5, 10, 20, 30 mV s^{-1} had been conducted in 6.0 M KOH electrolyte.

Because the contribution of blank NF to the capacitance is negligible (Figure S1a in the Supporting Information), the total capacitance primarily arises from the redox reaction of the loaded Co_3O_4. Figure 7a presents the CV curves of the Co_3O_4-modified electrode. The test was carried out under a fixed potential window, 0.1−0.6 V. As illustrated in the CV curves, two pairs of redox peaks appear, which are considered to arise from Co^{2+}/Co^{3+} reaction and the conversion between Co^{3+} and Co^{4+}, respectively.[8] The reaction could be presented as follows:[33,34]

$$Co_3O_4 + OH^- + H_2O \Leftrightarrow 3CoOOH + e^-$$

$$CoOOH + OH^- \Leftrightarrow CoO_2 + H_2O + e^-$$

dx.doi.org/10.1021/am500464n | ACS Appl. Mater. Interfaces 2014, 6, 6739−6747

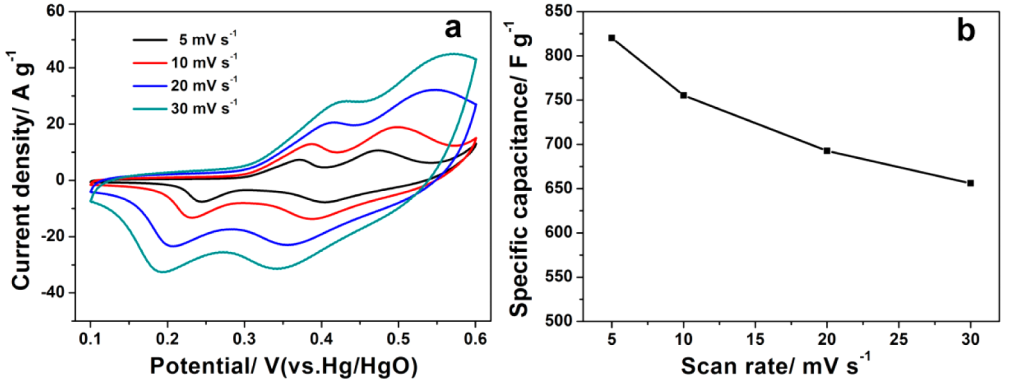

Figure 7. (a) CV curves of the Co_3O_4-modified electrode in 6.0 M KOH at different scan rates. (b) Specific capacitances at various scan rates.

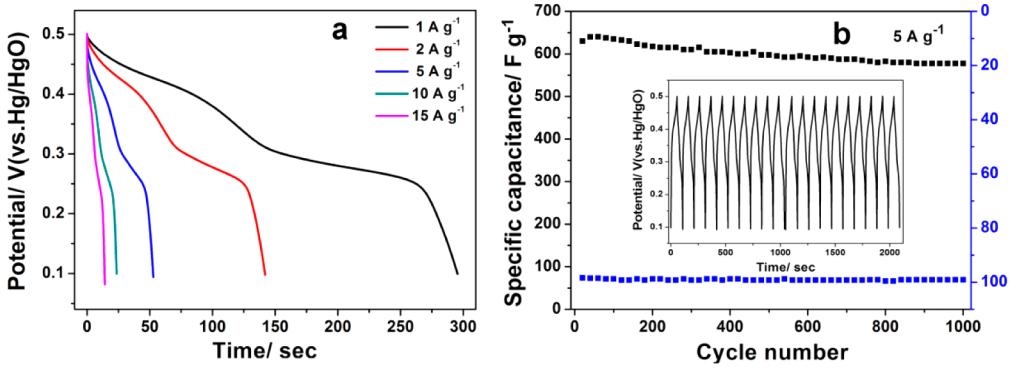

Figure 8. (a) Discharge curves of the Co_3O_4-modified electrode under the potential range from 0.1 to 0.5 V at different current densities. (b) Specific capacitance and coulombic efficiency (η) of the Co_3O_4-modified electrode as a function of cycle number.

The curves also indicate that the measured capacitance should be mainly based on redox reaction rather than EDLCs.[35] The asymmetric oxidation and reduction peaks result from the quasi-reversible redox process. In addition, ohmic resistance and polarization could contribute to this phenomenon through the diffusion of OH^- in porous electrode as well.[35] The SCs corresponding to the measurements at different scan rates were calculated by using the following equation:[36]

$$C = \frac{q_a + q_c}{2m\Delta V}$$

Where C is specific capacitance (SC), q_a and q_c are the charges on the anodic and cathodic scans, m is the mass of the electroactive material, and ΔV is the potential range of CV.

On the basis of the equation, we can easily obtain that SCs at the scan rates of 5, 10, 20, and 30 mV s^{-1} were 820, 755, 693, and 656 F g^{-1}, respectively. The prominent SCs most probably benefit from the porous structure of the obtained Co_3O_4. To reveal the change of SC with the increase of scan rate more obviously, a curve indicating the function between SC and scan rate was plotted as Figure 7b. It was found that SC decreases with the increase of scan rate, suggesting the measured capacitance is mainly associated with the redox reaction. A mechanism[37] proposed previously could be used to explain the phenomenon. At a low scan rate, both the inner and outer surface of the material could be reached, whereas with the increase of the scan rate, the diffusion of the ions might more likely happen on the outer rather than inner surface of the nanostructure. Nevertheless, the not sharp decrease of SC demonstrates that the nanostructure of the calcined sample might act as a buffering reservoir to accommodate OH^-,[38] which in turn shortens the path of the ionic transport and relieves the fading of SC.

Further evidence had been provided by a galvanostatic charge−discharge measurement for the practical application of the obtained material as a supercapacitor. The charge−discharge measurement was conducted under the potential range of 0.1−0.5 V, at different but constant current densities of 1, 2, 5, 10, and 15 A g^{-1}. As shown in Figure 8a, the two discharge flats of each curve correspond well to the two pairs of redox peaks in the CV curves, further confirming the pseudocapacitance property of the as-prepared Co_3O_4 nanomaterial. The SC values were calculated using the following equation:[39,40]

$$C = It/\Delta V$$

where ΔV represents the discharge potential range, I is the constant charge or discharge current density, and t is the corresponding discharge time.

Corresponding to the current densities of 1, 2, 5, 10, and 15 A g^{-1}, the SCs were calculated to be 739, 710, 660, 590, 533 F g^{-1}, respectively. Generally, the boost of current density would result in fading in the capacitance value,[3,41,42] possibly owing to the imposed mechanical stress generated from insertion and deinsertion of electrolyte ions.[43] It is exciting to find a 533 F g^{-1} value remained even at 15 A g^{-1} with a relatively high weight-loading (3.28 mg cm^{-2}),[12,13] which is significant for the practical use of the material as a supercapacitor. The pseudocapacitive properties obtained above reflect the advantage of the obtained 3D-nanonet hollow structured Co_3O_4 in turn. In addition, a comparison (Table S2 in the Supporting Information) between the 3D-nanonet hollow

dx.doi.org/10.1021/am500464n | ACS Appl. Mater. Interfaces 2014, 6, 6739−6747

structured Co_3O_4 in our work and the Co_3O_4 capacitive materials in current reports[5,12,16,44−48] has been made. The as-prepared Co_3O_4 material stands out because of the extremely simple synthetic method and relatively high capacitance.

To evaluate the cyclic stability of as-prepared Co_3O_4, a 1000-cycle charge−discharge assessment of our fabricated electrode was conducted under a current density of 5 A g^{-1}. As depicted in Figure 8b, less than 10 % loss in SC value is observed after the long-term cycling test, which is much better than the papers reported previously.[5,16] What's more, the coulombic efficiency, a vital certification of the feasibility of the redox process, remained nearly unchanged at ∼100%, indicating a feasible redox process generating from our obtained material. In other words, all the results above manifest that the long-lasting cycling test does no substainitial damage to the microstructure of the material, verifying the prominent electrochemical stability. Further evidence had been provided by EIS measurement.

EIS images of the electrode system before and after a long-term cycling measurement are presented in Figure 9 in the

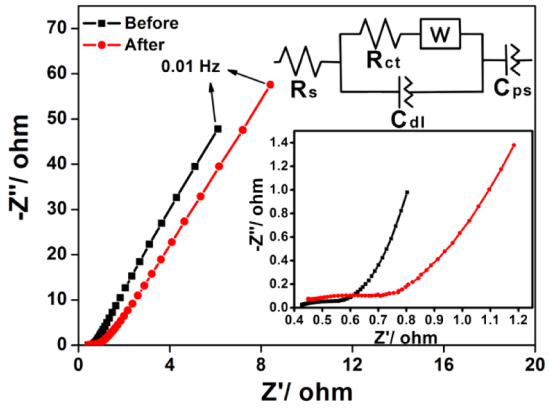

Figure 9. EIS plots of the as-synthesized Co_3O_4-modified electrode in 6.0 M KOH solution before and after a cycle test. The inset shows the equivalent circuit and the enlarged view of the high frequency region.

form of a Nyquist plot consisting of a small semicircle at the high frequency region and a deep-rising straight line at the low frequency region. At a high frequency, the diameter of the small semicircle reflects the charge-transfer resistance (R_{ct}),[49] whereas at a low frequency, the slope of the line corresponds to the diffusive resistance of the OH^- ions (Warburg impedance, W) within the Co_3O_4 electrode.[12] As we can see in the bottom inset of Figure 9, both the diameter of the semicircle and the slope of the line have changed after the cyclic test, which is most likely due to the repetitive mechanical stress during the charge−discharge process at high current density. However, the not apparent deviation is consistent with the slight fading of the capacitance and also reveals that the long-term cycling does not induce major degradation of the obtained microstructure. Also, a tiny bias of the start position, the intersection of curve at real part, is observed. Because the value indicates the resistance of the electrochemical system (R_s, including ionic resistance of electrolyte, contact resistance at the interface of electrolyte and electrode, and the intrinsic resistance of the calcined material),[50] the deviation phenomenon may result from the negligible change of the electrode system. To support what we had expressed above, a model (in the inset), consisting of R_s, R_{ct}, double layer capacitance C_{dl}, pseudocapacitance C_{ps}, and W, was exerted to fit the obtained spectra. The Co_3O_4-modified electrode exhibited very low R_s of 0.43 ohm and R_{ct} of 0.13 ohm before the cyclic test, which coincides well with the superior capacitance of the material. Also, the R_s of 0.45 ohm and R_{ct} of 0.26 ohm after the cycling measurement corresponds to the slight fading of the capacitance.

The energy density (E) and power density (P) were calculated from the charge−discharge measurements using the following equations:

$$E = \frac{1}{2}C(\Delta V)^2$$

$$P = \frac{E}{T}$$

where C is SC obtained at different current densities, ΔV and T are the corresponding potential window and discharging time, respectively.

To express the relationship clearly, a double-Y plot involving E and P against current density is displayed in Figure 10. As

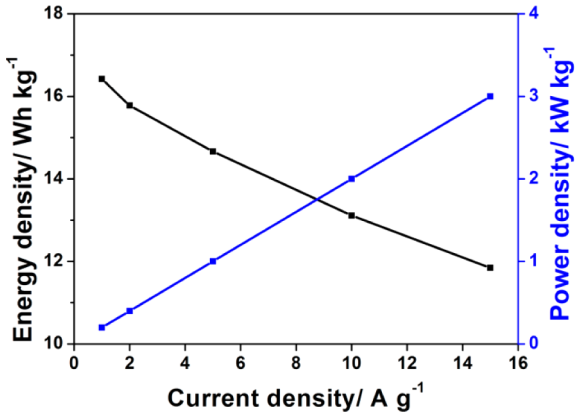

Figure 10. Specific energy and power density of the Co_3O_4-modified electrode as a function of current density.

shown in the image, our electroactive electrode exhibits an energy density of 16.42 Wh kg^{-1} at a power density of 0.2 kW kg^{-1}. Furthermore, even at a high power density of 3 kW kg^{-1}, our electrochemical system still has an energy density of 11.84 Wh kg^{-1}. All the results above have proven the prepared 3D-nanonet hollow structured Co_3O_4 to be a promising candidate for supercapacitor applications.

4. CONCLUSION

In summary, we have introduced a facile, low cost, and eco-friendly method for the synthesis of 3D-nanonet hollow structured Co_3O_4 with prominent pseudocapacitive properties. The electrochemical studies demonstrate unexpected specific capacitance and excellent energy and power density. In addition, the fabricated electrode exhibits outstanding cycling stability and enhanced rate capability. The superior cyclic and structural stability at a current density of 5 A g^{-1} with almost 100% coulombic efficiency enable our obtained material to be a promising candidate for supercapacitor applications. Furthermore, our work not only proposes a simple fabrication route for high capacitance hollow structured Co_3O_4 but also opens up a possible approach for obtaining other capacitive materials on a large scale.

■ ASSOCIATED CONTENT

Supporting Information

Illustration of the CV response of the blank NF and the capacitances of the materials obtained under different experimental conditions, TEM images of the as-prepared precursor and a comparison between 3D-nanonet hollow structured Co_3O_4 in our work and the Co_3O_4 capacitive materials in current reports about synthetic method and capacitance. This material is available free of charge via the Internet at http://pubs.acs.org.

■ AUTHOR INFORMATION

Corresponding Author

*D. Xiao. Tel: +86-28-85416029. Fax: +86-28-85415029. E-mail: xiaodan@scu.edu.cn.

Notes

The authors declare no competing financial interest.

■ ACKNOWLEDGMENTS

This work was financially supported by the Natural Science Foundation of China (Nos. 21177090, 21275104 and 21175094).

■ REFERENCES

(1) Wang, Y.; Cao, G. Developments in Nanostructured Cathode Materials for High-Performance Lithium-Ion Batteries. *Adv. Mater.* **2008**, *20*, 2251−2269.

(2) Gogotsi, Y.; Simon, P. True Performance Metrics in Electrochemical Energy Storage. *Science* **2011**, *334*, 917−918.

(3) Winter, M.; Brodd, R. J. What are Batteries, Fuel Cells, and Supercapacitors? *Chem. Rev.* **2004**, *104*, 4245−4270.

(4) Wei, T. Y.; Chen, C. H.; Chien, H. C.; Lu, S. Y.; Hu, C. C. A Cost-Effective Supercapacitor Material of Ultrahigh Specific Capacitances: Spinel Nickel Cobaltite Aerogels from an Epoxide-Driven Sol-Gel Process. *Adv. Mater.* **2010**, *22*, 347−351.

(5) Du, W.; Liu, R.; Jiang, Y.; Lu, Q.; Fan, Y.; Gao, F. Facile Synthesis of Hollow Co_3O_4 Boxes for High Capacity Supercapacitor. *J. Power Sources* **2012**, *227*, 101−105.

(6) Tian, X. Q.; Cheng, C. M.; Qian, L.; Zheng, B.; Yuan, H.; Xie, S.; Xiao, D.; Choi, M. M. Microwave-Assisted Non-Aqueous Homogenous Precipitation of Nanoball-Like Mesoporous α-$Ni(OH)_2$ as a Precursor for NiO_x and Its Application as a Pseudocapacitor. *J. Mater. Chem.* **2012**, *22*, 8029−8035.

(7) Liang, Y.; Wang, H.; Casalongue, H. S.; Chen, Z.; Dai, H. TiO_2 Nanocrystals Grown on Graphene as Advanced Photocatalytic Hybrid Materials. *Nano Res.* **2010**, *3*, 701−705.

(8) Cao, L.; Xu, F.; Liang, Y. Y.; Li, H. L. Preparation of the Novel Nanocomposite Co $(OH)_2$/Ultra-Stable Y Zeolite and Its Application as a Supercapacitor with High Energy Density. *Adv. Mater.* **2004**, *16*, 1853−1857.

(9) Liu, J.; Jiang, J.; Cheng, C.; Li, H.; Zhang, J.; Gong, H.; Fan, H. J. Co_3O_4 Nanowire@ MnO_2 Ultrathin Nanosheet Core/Shell Arrays: A New Class of High-Performance Pseudocapacitive Materials. *Adv. Mater.* **2011**, *23*, 2076−2081.

(10) Wei, T. Y.; Chen, C. H.; Chang, K. H.; Lu, S. Y.; Hu, C. C. Cobalt Oxide Aerogels of Ideal Supercapacitive Properties Prepared with An Epoxide Synthetic Route. *Chem. Mater.* **2009**, *21*, 3228−3233.

(11) Cheng, J.; Chen, X.; Wu, J. S.; Liu, F.; Zhang, X.; Dravid, V. P. Porous Cobalt Oxides with Tunable Hierarchical Morphologies for Supercapacitor Electrodes. *CrystEngComm* **2012**, *14*, 6702−6709.

(12) Meher, S. K.; Rao, G. R. Ultralayered Co_3O_4 for High-Performance Supercapacitor Applications. *J. Phys. Chem. C* **2011**, *115*, 15646−15654.

(13) Yang, L.; Cheng, S.; Ding, Y.; Zhu, X.; Wang, Z. L.; Liu, M. Hierarchical Network Architectures of Carbon Fiber Paper Supported Cobalt Oxide Nanonet for High-Capacity Pseudocapacitors. *Nano Lett.* **2011**, *12*, 321−325.

(14) Yuan, C.; Yang, L.; Hou, L.; Li, J.; Sun, Y.; Zhang, X.; Shen, L.; Lu, X.; Xiong, S.; Lou, X. W. D. Flexible Hybrid Paper Made of Monolayer Co_3O_4 Microsphere Arrays on rGO/CNTs and Their Application in Electrochemical Capacitors. *Adv. Funct. Mater.* **2012**, *22*, 2560−2566.

(15) Yuan, C.; Yang, L.; Hou, L.; Shen, L.; Zhang, X.; Lou, X. W. D. Growth of Ultrathin Mesoporous Co_3O_4 Nanosheet Arrays on Ni Foam for High-Performance Electrochemical Capacitors. *Energy Environ. Sci.* **2012**, *5*, 7883−7887.

(16) Wang, D.; Wang, Q.; Wang, T. Morphology-Controllable Synthesis of Cobalt Oxalates and Their Conversion to Mesoporous Co_3O_4 Nanostructures for Application in Supercapacitors. *Inorg. Chem.* **2011**, *50*, 6482−6492.

(17) Meher, S. K.; Justin, P.; Ranga Rao, G. Microwave-Mediated Synthesis for Improved Morphology and Pseudocapacitance Performance of Nickel Oxide. *ACS Appl. Mater. Interfaces* **2011**, *3*, 2063−2073.

(18) Yuan, C.; Li, J.; Hou, L.; Yang, L.; Shen, L.; Zhang, X. Facile Template-Free Synthesis of Ultralayered Mesoporous Nickel Cobaltite Nanowires towards High-Performance Electrochemical Capacitors. *J. Mater. Chem.* **2012**, *22*, 16084−16090.

(19) Huang, H.; Zhu, W.; Tao, X.; Xia, Y.; Yu, Z.; Fang, J.; Gan, Y.; Zhang, W. Nanocrystal-Constructed Mesoporous Single-Crystalline Co_3O_4 Nanobelts with Superior Rate Capability for Advanced Lithium-Ion Batteries. *ACS Appl. Mater. Interfaces* **2012**, *4*, 5974−5980.

(20) Roginskaya, Y. E.; Morozova, O.; Lubnin, E.; Ulitina, Y. E.; Lopukhova, G.; Trasatti, S. Characterization of Bulk and Surface Composition of $Co_xNi_{1-x}O_y$ Mixed Oxides for Electrocatalysis. *Langmuir* **1997**, *13*, 4621−4627.

(21) Marco, J.; Gancedo, J.; Gracia, M.; Gautier, J.; Rıos, E.; Berry, F. Characterization of the Nickel Cobaltite, $NiCo_2O_4$, Prepared by Several Methods: An XRD, XANES, EXAFS, and XPS Study. *J. Solid State Chem.* **2000**, *153*, 74−81.

(22) Xu, R.; Zeng, H. C. Dimensional Control of Cobalt-Hydroxide-Carbonate Nanorods and Their Thermal Conversion to One-Dimensional Arrays of Co_3O_4 Nanoparticles. *J. Phys. Chem. B* **2003**, *107*, 12643−12649.

(23) He, T.; Chen, D.; Jiao, X.; Wang, Y. Co_3O_4 Nanoboxes: Surfactant-Templated Fabrication and Microstructure Characterization. *Adv. Mater.* **2006**, *18*, 1078−1082.

(24) Klissurski, D.; Uzunova, E. Synthesis of Nickel Cobaltite Spinel from Coprecipitated Nickel-Cobalt Hydroxide Carbonate. *Chem. Mater.* **1991**, *3*, 1060−1063.

(25) LoáJacono, M. Preparation and Characterisation of Cobalt-Copper Hydroxysalts and Their Oxide Products of Decomposition. *J. Chem. Soc. Faraday Trans.* **1992**, *88*, 311−319.

(26) Peng, Q.; Dong, Y.; Li, Y. ZnSe Semiconductor Hollow Microspheres. *Angew. Chem., Int. Ed.* **2003**, *42*, 3027−3030.

(27) Wu, C.; Xie, Y.; Lei, L.; Hu, S.; OuYang, C. Synthesis of New-Phased VOOH Hollow "Dandelions" and Their Application in Lithium-Ion Batteries. *Adv. Mater.* **2006**, *18*, 1727−1732.

(28) Guo, L.; Liang, F.; Wen, X.; Yang, S.; He, L.; Zheng, W.; Chen, C.; Zhong, Q. Uniform Magnetic Chains of Hollow Cobalt Mesospheres from One-Pot Synthesis and Their Assembly in Solution. *Adv. Funct. Mater.* **2007**, *17*, 425−430.

(29) Gao, J.; Zhang, B.; Zhang, X.; Xu, B. Magnetic-Dipolar-Interaction-Induced Self-Assembly Affords Wires of Hollow Nanocrystals of Cobalt Selenide. *Angew. Chem.* **2006**, *118*, 1242−1245.

(30) Zhu, T.; Chen, J. S.; Lou, X. W. Shape-Controlled Synthesis of Porous Co_3O_4 Nanostructures for Application in Supercapacitors. *J. Mater. Chem.* **2010**, *20*, 7015−7020.

(31) Xiao, J.; Yang, S. Sequential Crystallization of Sea Urchin-Like Bimetallic (Ni, Co) Carbonate Hydroxide and Its Morphology Conserved Conversion to Porous $NiCo_2O_4$ Spinel for Pseudocapacitors. *RSC Adv.* **2011**, *1*, 588−595.

(32) Simon, P.; Gogotsi, Y. Materials for Electrochemical Capacitors. *Nat. Mater.* **2008**, *7*, 845−854.

(33) Casella, I. G.; Gatta, M. Study of The Electrochemical Deposition and Properties of Cobalt Oxide Species in Citrate Alkaline Solutions. *J. Electroanal. Chem.* **2002**, *534*, 31−38.
(34) Švegl, F.; Orel, B.; Hutchins, M.; Kalcher, K. Structural and Spectroelectrochemical Investigations of Sol-Gel Derived Electrochromic Spinel Co_3O_4 Films. *J. Electrochem. Soc.* **1996**, *143*, 1532−1539.
(35) Mondal, C.; Ganguly, M.; Manna, P. K.; Yusuf, S.; Pal, T. Fabrication of Porous β-$Co(OH)_2$ Architecture at Room Temperature: A High Performance Pupercapacitor. *Langmuir* **2013**, *29*, 9179−9187.
(36) Song, R. Y.; Park, J. H.; Sivakkumar, S.; Kim, S. H.; Ko, J. M.; Park, D. Y.; Jo, S. M.; Kim, D. Y. Supercapacitive Properties of Polyaniline/Nafion/Hydrous RuO_2 Composite Electrodes. *J. Power Sources* **2007**, *166*, 297−301.
(37) Pang, H.; Zhang, B.; Du, J.; Chen, J.; Zhang, J.; Li, S. Porous Nickel Oxide Nanospindles with Huge Specific Capacitance and Long-Life Cycle. *RSC Adv.* **2012**, *2*, 2257−2261.
(38) Wang, D. W.; Li, F.; Liu, M.; Lu, G. Q.; Cheng, H. M. 3D Aperiodic Hierarchical Porous Graphitic Carbon Material for High-Rate Electrochemical Capacitive Energy Storage. *Angew. Chem.* **2008**, *120*, 379−382.
(39) Yuan, C.; Li, J.; Hou, L.; Zhang, X.; Shen, L.; Lou, X. W. D. Ultrathin Mesoporous $NiCo_2O_4$ Nanosheets Supported on Ni Foam as Advanced Electrodes for Supercapacitors. *Adv. Funct. Mater.* **2012**, *22*, 4592−4597.
(40) Liu, M. C.; Kong, L. B.; Lu, C.; Li, X. M.; Luo, Y. C.; Kang, L. A Sol-Gel Process for Fabrication of $NiO/NiCo_2O_4/Co_3O_4$ Composite with Improved Electrochemical Behavior for Electrochemical Capacitors. *ACS Appl. Mater. Interfaces* **2012**, *4*, 4631−4636.
(41) Meher, S. K.; Justin, P.; Rao, G. R. Nanoscale Morphology Dependent Pseudocapacitance of NiO: Influence of Intercalating Anions during Synthesis. *Nanoscale* **2011**, *3*, 683−692.
(42) Liang, Y.; Schwab, M. G.; Zhi, L.; Mugnaioli, E.; Kolb, U.; Feng, X.; Müllen, K. Direct Access to Metal or Metal Oxide Nanocrystals Integrated with One-Dimensional Nanoporous Carbons for Electrochemical Energy Storage. *J. Am. Chem. Soc.* **2010**, *132*, 15030−15037.
(43) Meher, S. K.; Rao, G. R. Enhanced Activity of Microwave Synthesized Hierarchical MnO_2 for High Performance Supercapacitor Applications. *J. Power Sources* **2012**, *215*, 317−328.
(44) Xia, X. H.; Tu, J. P.; Zhang, Y. Q.; Mai, Y. J.; Wang, X. L.; Gu, C. D.; Zhao, X. B. Freestanding Co_3O_4 Nanowire Array for High Performance Supercapacitors. *RSC Adv.* **2012**, *2*, 1835−1841.
(45) Du, H.; Jiao, L.; Wang, Q.; Yang, J.; Guo, L.; Si, Y.; Wang, Y.; Yuan, H. Facile Carbonaceous Microsphere Templated Synthesis of Co_3O_4 Hollow Spheres and Their Electrochemical Performance in Supercapacitors. *Nano Res.* **2013**, *6*, 87−98.
(46) Liao, M.; Liu, Y.; Hu, Z.; Yu, Q. Novel Morphologic Co_3O_4 of Flower-Like Hierarchical Microspheres as Electrode Material for Electrochemical Capacitors. *J. Alloys Compd.* **2013**, *562*, 106−110.
(47) Xia, X. H.; Tu, J. P.; Wang, X. L.; Gu, C. D.; Zhao, X. B. Mesoporous Co_3O_4 Monolayer Hollow-Sphere Array as Electrochemical Pseudocapacitor Material. *Chem. Commun.* **2011**, *47*, 5786−5788.
(48) Xia, X. H.; Tu, J. P.; Mai, Y. J.; Wang, X. L.; Gu, C. D.; Zhao, X. B. Self-Supported Hydrothermal Synthesized Hollow Co_3O_4 Nanowire Arrays with High Supercapacitor Capacitance. *J. Mater. Chem.* **2011**, *21*, 9319−9325.
(49) Liu, J.; Jiang, J.; Bosman, M.; Fan, H. J. Three-Dimensional Tubular Arrays of MnO_2-NiO Nanoflakes with High Areal Pseudocapacitance. *J. Mater. Chem.* **2012**, *22*, 2419−2426.
(50) Zhou, C.; Zhang, Y.; Li, Y.; Liu, J. Construction of High-Capacitance 3D CoO@Polypyrrole Nanowire Array Electrode for Aqueous Asymmetric Supercapacitor. *Nano Lett.* **2013**, *13*, 2078−2085.